VIII International Conference on Fracture Mechanics of Concrete and Concrete Structures
FraMCoS-8
J.G.M. Van Mier, G. Ruiz, C. Andrade, R.C. Yu and X.X. Zhang (Eds)

UPGRADING THE PUSH-OFF TEST TO STUDY THE MECHANISMS OF SHEAR TRANSFER IN FRC ELEMENTS

JAVIER ECHEGARAY-OVIEDO[*], JUAN NAVARRO-GREGORI[*], ESTEFANIA CUENCA[*] AND PEDRO SERNA[*]

[*] Universitat Politècnica de València (UPV)
ICITECH – ETS de Ingenieros de Caminos, Canales y Puertos
Edificio 4G. Camino de Vera s/n, 46071, Valencia, Spain
e-mail: jaecov@posgrado.upv.es,
e-mail: juanagre@cst.upv.es; escueas@upvnet.upv.es; pserna@cst.upv.es, www.icitech.upv.es

Key words: Push-off test, Aggregate Interlock, Fiber Reinforced Concrete, Shear Transfer.

Abstract: In this paper an upgrading of the push-off test in pre-cracked specimens is presented. The test is performed under conditions of crack control both in the pre-cracking and in the push-off stages. To this end, transversal forces to control the crack opening are introduced. Additionally, this confinement system avoids unnecessary movements that may introduce strains in the specimen. It is also included the methodology to perform the pre-cracking of the specimens prior to the push-off test. Specimens of 40 MPa of concrete compressive strength are used with two types of steel fibers type as well as with transverse reinforcement. It can be concluded that it is possible to perform the push-off test under crack control as it is shown with the results of crack width obtained with different measurement techniques. Different types of behavior after cracking can be detected such as hardening or the evolution of post-cracking residual stresses.

1 INTRODUCTION

It is well known that the shear failure of reinforcement concrete elements is brittle. The addition of steel fibers to the concrete mixture improves the tensile behavior and ductility, as well as it provides a good crack control [1]. Also, steel fibers improve the shear behavior of structural elements increasing their shear load capacity, and ductility [2].

The push-off test (Fig. 1a) has been used to study the mechanisms of shear transfer [3-10]. Some researchers pre-crack the specimen before performing the push-off test [5-10]. Pre-cracking can be achieved by first placing the specimen horizontally (Fig. 1b), and then a line load at the top and at the bottom face of the specimen is applied. Finally, the specimen is placed vertically, and the push-off test is then carried out.

The shear strength of the specimen depends on the contribution of both the concrete and the shear reinforcement. Aggregate interlock, or crack shear friction, has a significant contribution to the concrete shear capacity [8].

Walraven [7], analyzed the phenomenon of aggregate interlock by means of push-off tests, and proposed a model validated with his own experimental results. This model assumes that concrete consists of a rigid perfectly plastic paste and rigid spherical aggregates of various sizes intruded into this paste. After the formation of a crack plane, for normal concrete strength, the aggregates tend to be pulled out from the cement paste with the propagation of cracks. The crack grows through the paste an around the aggregate. These spherical aggregates effectively provide aggregate interlock between the paste and the

aggregate. Protruded aggregates sliding against the paste generate normal and shear stresses due to plastic deformation of the paste. The simplified version of Walraven's model is based on expressions [1] and [2], which relate the shear (τ) and normal (σ) stresses with the slip (Δ) and the crack width (w):

$$\sigma = -\frac{f_{cu}}{20} + [1{,}35w^{-0{,}63} + (0{,}191w^{-0{,}552} - 0{,}15)f_{cu}]\,\Delta \quad (1)$$

$$\tau = -\frac{f_{cu}}{30} + [1{,}80w^{-0{,}80} + (0{,}234w^{-0{,}707} - 0{,}20)f_{cu}]\Delta \quad (2)$$

where f_{cu} is the concrete cube compressive strength.

In the last decades new types of concrete have been used, like high strength concrete (HSC), self-compacting concrete (SCC), or fiber reinforced concrete (FRC) among others. In these concrete materials the aggregate interlock phenomenon may be different compared to conventional concrete.

In the case of HSC, Walraven [9] introduced the C parameter (C < 1), which reduces the stresses due to the aggregate fracture. Indeed this parameter should be considered as a general roughness reduction factor. If all particles break there is always some shear capacity left thanks to the natural unevenness of the crack face.

On the other hand, Kim [10], carried out experimental tests on push-off specimens made with SCC and high strength concrete (f_c > 70MPa). His results confirmed that concrete shear strength is highly related to the amount of aggregate fracture at small crack widths when crack slip initiates. Moreover, concrete mixtures containing river gravel exhibited higher aggregate interlock compared to those containing crushed limestone aggregate. The fact that SCC has a lower volume of coarse aggregate than conventional concrete (CC) should imply lower shear strength. However, there are several authors [11, 12], who have shown that the shear strength is similar to CC, if both materials have similar granular skeleton.

There is a lack of information in the literature about the real mechanisms of shear transfer in FRC elements. It remains unclear the role that steel fibers play right at the cracks. Cuenca et al. [13] studied the shear behavior of push-off specimens made with different amounts of fibers (0, 40 and 60 kg/m^3) and pre-cracked width, and compared the results with conventional concrete. They found out that the peak load increases with the amount of steel fibers and the reinforcement rebars presence, but is much reduced when specimens is pre-cracked.

Boulekbach et al. [14] studied the behavior of prismatic specimens of 10x10x35cm of several concrete strengths (30, 60 and 80 MPa), reinforced with hooked-end steel fibers with three volume contents of fibers (0%, 0.5% and 1%) and two different aspects ratio (65 and 80). They found out that the first way to improve the shear strength consists of increasing the concrete compressive strength. The second way can be obtained with the addition of steel fibers; an increment of 44% is obtained for a fiber volume content of 0.5%, and 65% for a content of 1%. Finally, the use of an aspect ratio ranging from 65 to 80 has shown a slight influence on the shear strength (5%).

2 RESEARCH SIFNIFICANCE

In this study an improvement of the push-off test in pre-cracked specimens is presented. With this method is possible to control the crack width in both, the pre-cracking and the push-off stages.

This kind of test allows the study of specimens under direct shear controlling the maximum crack width. Thus, both shear and normal stresses mainly depend on the slip displacement (or shear displacement).

3 METHODOLOGY

3.1 The push-off test concept

The push-off test is based on the idea of applying an axial force (P) to produce a pure shear on a plane of the specimen (shear plane). To make this possible, a special specimen is used. This is formed by two L blocks, and the shear plane is defined by the plane that

connects these two blocks.

It is important to outline that the shear plane direction must be coincident with the load direction. Thus, the cracking and failure of the specimen is produced along the shear plane. A simplified representation of this concept is shown in Fig. 1a

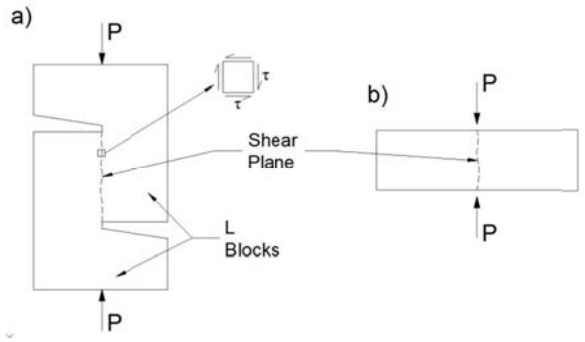

Figure 1: The push-off test concept.

3.2 Push-off test upgrading

The upgrading of the push-off test is based on the idea of controlling the crack width by means of a rigid steel frame that confines the specimen (Fig. 2).

This frame is formed by two steel plates jointed each other with four steel bars (ϕ25 mm). Each bar has two bolts on one extreme and one bolt in the other one. On one side of the push-off specimen the plate is rigidly jointed to it. On the other side, there is a special mechanism which is rigidly jointed to it (see Fig. 2). The aim of this mechanism is to avoid frictional forces between the plates and the specimen. Therefore, it is possible to guarantee that it does not exist bending on the bars, and also avoids relative displacements between the plates. For that reason the four bars experiment only axial forces. Thus, it is possible to evaluate by means of electrical strain gauges on the bars. Finally, the crack width can be controlled by adjusting the distances between the mechanisms and the last plate.

This mechanism to confine the specimen is the key of this new method, and it makes a difference compared with push-off speciments tested by previous authors [6 and 7], that try to control the crack width, by using a rigid steel frame.

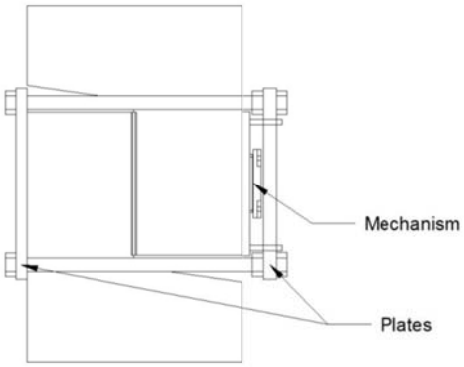

Figure 2: Steel frame to confine the push-off specimen.

3.3 Pre-cracking

From now on, it is defined as F1 the face of the specimen in which concrete is cast, while F2 is the opposite face in contact with the formwork. F3 and F4 are defined as the top and the bottom faces of the specimen respectively; this is shown in Fig 3.

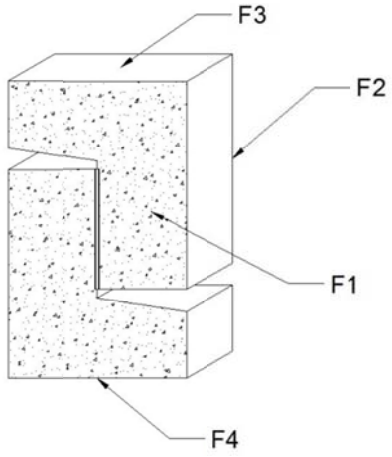

Figure 3: Specimen's faces definition.

All specimens are intentionally cracked along the shear plane before carrying out the push-off test. To this aim the specimen is placed horizontally. Then, a steel knife is provided along the F1 and F2 surfaces. In order to create a plane of weakness, along the shear plane, a couple of notches are done.

Specimen rotations may occur along the line load during the pre-cracking operation. To solve this inconvenience some springs have been included to stabilize the specimen. The stiffness of the springs (k) must be chosen in

order to avoid a significant bending effect positive or negative, once the crack is formed. If the stiffness is too low (k→0), negative bending effect appears. In the opposite case, (k→∞), positive effect appears (Fig. 4).

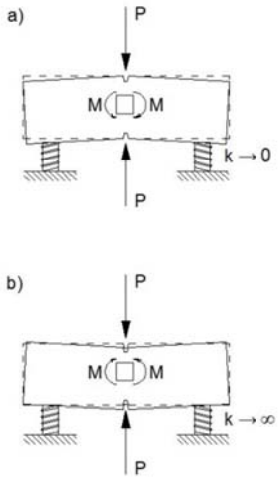

Figure 4: Function of the springs. a) Negative bending effect. a) Positive bending effect.

This test is carried out using six LVDT's, to measure vertical displacements (1 to 6) and two LVDT's to measure cracks width (w1 and w2), as it is shown in Fig 4. This setup allows having three targets points on each L block. For this reason it is possible to know the displacements of the plane which defines the surface of the specimen.

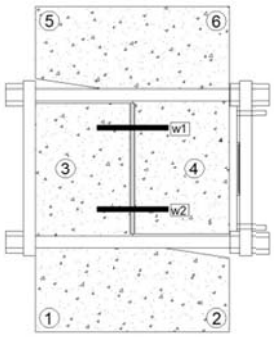

Figure 5: Disposition of the LVDT's during pre-cracking.

As it can be seen on Fig. 4, points 1, 2 and 3 define one block, and points 4, 5 and 6 the other one.

The specimen is carefully horizontally placed under a hydraulic jack which applies a line load along the notch. The load is increased until a crack forms in the shear plane. A general disposition of this test instrumentation is shown in Fig. 6.

Figure 6: Pre-crack position.

3.4 Push-off test

Once the specimen is pre-cracked along the shear plane, it is placed in vertical position to carry out the push-off test. This operation is risky, because if the specimen is placed in a wrong position the results can be totally wrong.

For this reason, different ways to place the specimen have been tested. The technique which better results provided consists of a steel plate located at the F4 face of the specimen. On this plate, a steel piece is fixed and allows the specimen sliding.

When the specimen is on the correct position, another steel piece is placed on F3. Over this plate the load cell is included, so the boundary conditions are similar in both, F3 and F4 faces of the specimen. Then, specimen is loaded until a slip displacement of 5 mm is reached. During this phase, both crack width and slip along the shear plane are measured. For this purpose four LVDT's are mounted on brackets to attach the specimen on both sides of the shear plane (see Fig. 7), two to measure vertical displacements and two to measure crack widths. This configuration is also repeated on F2 face. With the aim to know the relative vertical displacement between the two plates of the steel frame, they are instrumented with four LVDT's.

Also during this stage, strain measurements of the external reinforcement bars are taken by

means of electrical gauges. The aim of these is to know the normal stresses (σ) in an indirect way. The electrical gauges are put in the middle of the bar as shown in Fig. 7.

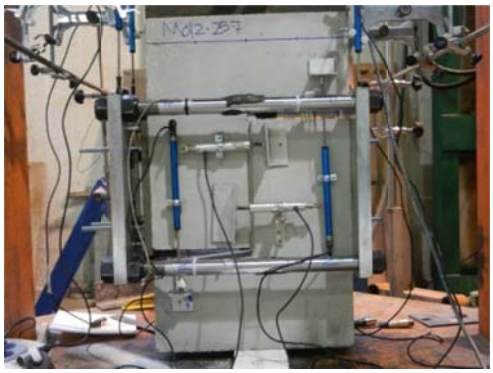

Figure 7: Disposition of the LVDT's and strain gages

3.5 Micro-photographs

The idea of using micro-photographs to obtain measurements is not something new. Given the fact that the crack widths are very small, the use of micro-photographs may be a good alternative solution of measurement.

In the present study, the following steps have been taken to use this technique: first, four target points; two at each face of the specimen are selected. These four points are placed at 5 cm from the steel bars, and in the exact location where LVDT's measure the crack width (see Fig. 8). Then, photographs of each point before and after pre-cracking are taken. Finally, another group of photographs on the same four points are taken at failure

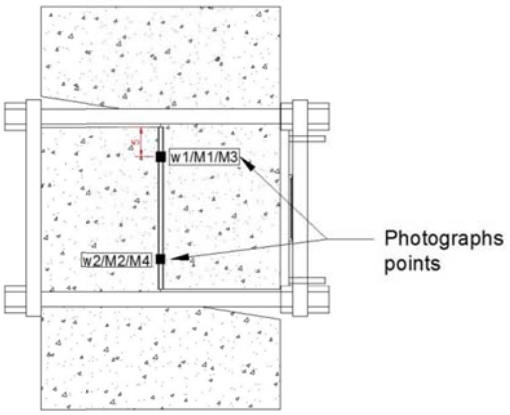

Figure 8: Position of the four targets points on the specimen: M1 and M2 on F1 face. M3 and M4 on F2 face.

4 EXPERIMENTAL PROGRAM

4.1 Aim of the experimental program

Several specimens were tested in order to calibrate and to solve difficulties derived from the new test method proposed.

To this end, four specimens were made with normal strength concrete ($f_c \approx 40$MPa). One of them was reinforced with stirrups and the others included two types of steel fibers (normal and high strength). In Table 1, the references and the properties of the specimens are shown.

Table 1: References of the specimens.

Specimen	Reinforcement	Quantity	Concrete
RS-50-BN	Fiber 65/35-BN	1	H1
CR-30-BN	Fiber 65/35-BN	1	H2
CR-50-BP	Fiber 80/30-BP	1	H3
CS-F8	Stirrup 2ϕ8 mm	1	H4

4.2 Materials

The specimens were cast with self-compacting concrete. A Bolomey reference curve (with a=21 parameter) was selected to have a minimum of fines content to guarantee the required flowability, and thus avoiding any segregation risk. A good theoretical agreement was obtained (Fig. 9).

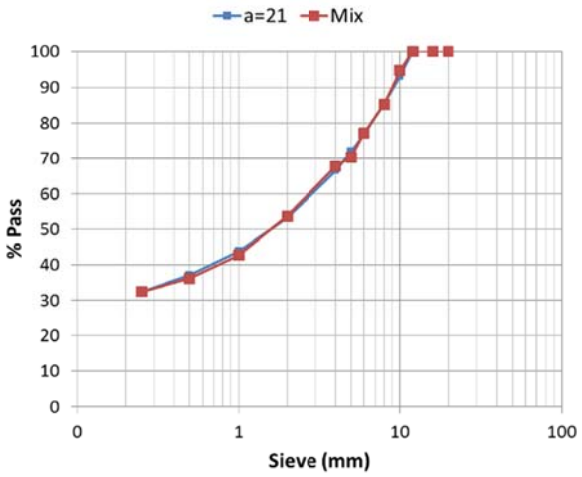

Figure 9: Particle size distribution.

Cement (CEM II/B-V 42,5R) was used for the concrete mixture. Also superplasticizer to achieve a self-compacting concrete was

employed.

Two different types of hooked-end steel fibers from Bekaert© were used. One of them was *normal strength*, low carbon fiber (BN) with a tensile strength of 1225 MPa. The other was *high strength*, high carbon (BP) with a tensile strength of 3070 MPa. Each type of fiber was referenced by its aspect ratio (length/diameter), its length (in mm) and the steel strength level according with the following notation:

{aspect ratio} / {length (in mm)} BN or BP

The mix proportions for 1 m^3 and the value of the Slump flow (S.F.) at 9 minutes after the superplasticizer was introduced, are shown in Table 2. Also, in this table the experimental results of the concrete strength are shown.

Table 2: Concrete dosages (kg/m^3).

	H1	H2	H3	H4
Cement	350	350	350	350
Water	189	201	204	210
Crush Sand	0	999	990	992
River Sand	1011	0	0	0
Gravel 4/7	191	191	190	191
Gravel 7/12	603	603	600	601
Filler	60	0	0	0
Fibers	50	30	50	0
Admixture	5,25	5,3	7,9	4,9
S. F. (mm)	600	400	440	480
f_c	50.49	50.13	52.34	51.37

4.2 Specimen

The geometry of the specimen (Fig. 10) that was used in the experimental program is quite similar to the one used by other authors [5, 6, 7 and 13]. The differences in geometry can be seen in Table 3.

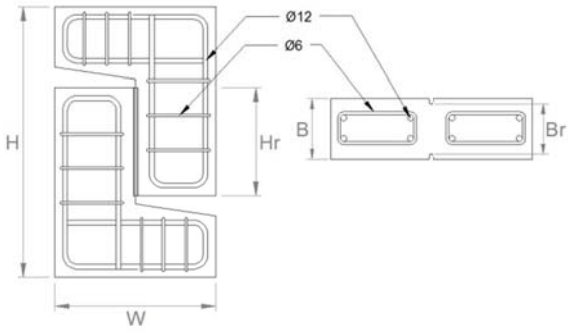

Figure 10: Geometry of the specimen.

Table 3: Specimens dimensions used by different authors.

Dimen. (mm)	Mattock (1969)	Paulay (1970)	Walraven (1981)	Cuenca (2010)	Ours (2012)
H	546.1	457.2	600	670	670
H_r	254	190.5	300	250	260
W	254	304.8	400	400	400
B	127	152.4	120	120	120
B_r	127	114.3	120	110	100

5 EXPERIMENTAL RESULTS

5.1 Pre-cracking

On this section, the results of the pre-cracking process are presented. In Fig. 11 the experimental results without the springs are shown. And in Fig. 12 the experimental results are shown when the springs were introduced.

In Fig. 11, it is shown the vertical displacements of the six LVDT's on "x" axis and load applied on "y" axis. Analyzing the curve, it can be observed how the specimen rotates around the knife. This is because points 1 and 3 go to negatives values, while point 2 goes to a positive value. And this behavior is more evident after the specimen is pre-cracked.

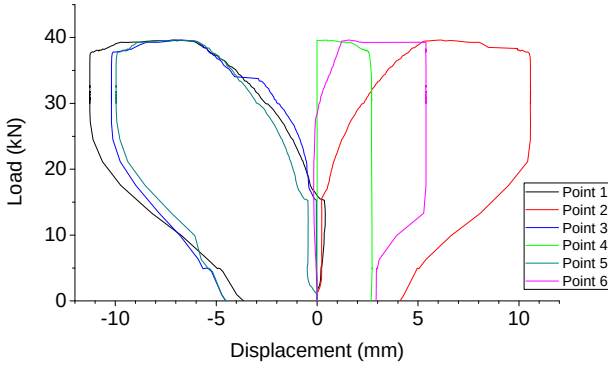

Figure 11: Example curve of pre-cracking process without springs.

A better behavior was obtained by introducing the springs mentioned in section 3.3. An example of this is shown in Fig 12.

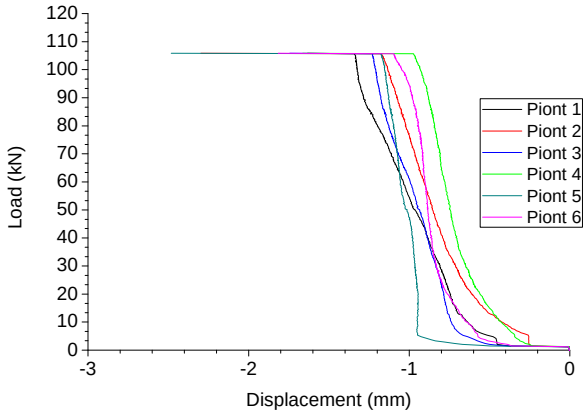

Figure 12: Example curve with springs during the pre-cracking process.

In Fig. 12 it can be seen how the six LVDT's go to negative values. This indicates, in one hand, that the specimen does not experiment any rotation around the knife. On the other hand, the stiffness of the springs is according to our necessities, because the differences between the six LVDT's measurements show a low scatter of results.

5.2 Push-off

The shear behavior was analyzed by means of the crack width (crack opening) or the slip (shear displacement) versus the shear applied during the push-off tests. A general example of one of these is presented in Fig. 13. It can be seen a different shear behavior between the river sand (RS-50-BN), the crush sand (CS-30-BN), the crush sand with BP fibers (CS-50-BP) specimens, and the crush sand reinforcement (CS-F8).

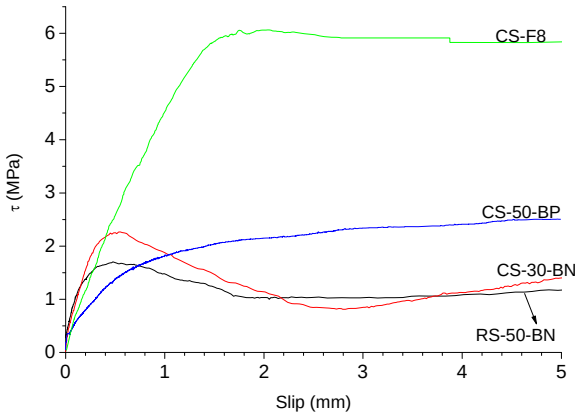

Figure 13: Example curve of the first pre-cracking process.

The curve RS-50-BN (black line) shows a residual stress, while CS-30-BN (red line) shows a hardening effect. The reason for the residual stress was that the distance between the two plates was too big (3.5 mm) so the specimen (RS-50-BN) was not confined by the plates. For this reason in the others specimens [(CS-30-BN) and (CS-50-BP)] the distance between the two plates was reduced to 1 mm and 0.5 mm respectively.

In the case of the reinforcement specimen CS-F8 (green line), the best behavior of all specimens was obtained. This can be seen on the value of the shear stress, because in this specimen it was around 6 MPa. And it was kept constant until the end of the test.

5.3 Micro-photographs

The results showed here were obtained from the specimen CS-50-BP, by following the methodology described in section 3.5. The general procedure was shown in Fig. 14. Here it is shown point M4, before and after pre-cracking and at failure.

The different values of the whole process are summarized in Table 4. Here, the *initial length* is defined as the width of the notch. *After pre-cracking,* means the length of the notch when the pre-cracking process is finished. And the column name *failure* is referred to the length of the notch at the

failure.

a)

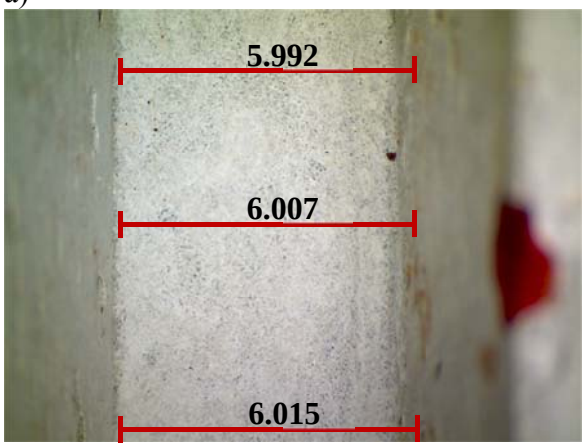

b)

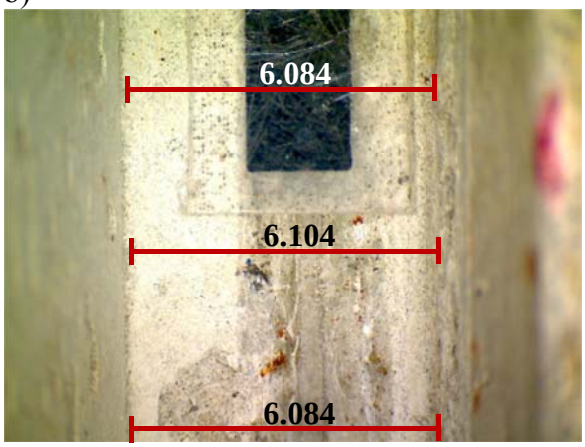

c)

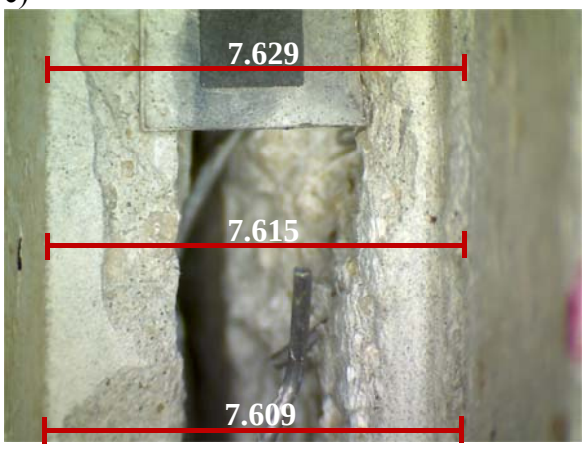

Figure 14: Photographs obtained with the microscope at point M4. a) Before pre-cracking. b) After pre-cracking. c) Failure.

Table 4: Photography measurements.

Point	Initial Length	After Pre-crack	Crack width	Failure	Crack width
	[mm]	[mm]	[mm]	[mm]	[mm]
M1	6.009	6.057	0.047	6.772	0.763
M2	6.010	6.050	0.040	7.106	1.096
M3	6.005	6.054	0.049	6.959	0.955
M4	6.005	6.091	0.086	7.618	1.613

So the crack width at the end of the pre-crack process was obtained by subtracting the value of the initial length from the value corresponding to the after pre-cracking. The same concept is followed to obtain the final crack width.

As a final check, in Table 5 the measurements obtained with the LVDT's and the total distance it is compared. The *Total distance* is obtained as the sum of the crack width taken from the photographs with the microscope and the increase of the bar length (ΔL). To obtain the value of ΔL, the equation 3 is used, where the bar strain (ε) was experimentally obtained and ($L = 440\ mm$) represents the original length of each bar (). Finally, the column *Error* shows the ratio between the LVDT's measurements and the Total distance.

$$\Delta L = \varepsilon \times L \qquad (3)$$

Table 5: Different measurements obtained from the test.

Point	LVDT's	Crack width	ΔL	Total Distance	Error
	[mm]	[mm]	[mm]	[mm]	[%]
M1	1.034	0.703	0.209	0.912	0.908
M2	1.762	1.105	0.292	1.397	0.793
M3	1.034	0.635	0.112	0.747	1.527
M4	1.641	0.971	0.179	1.151	0.701

5.4 Study of the crack surface

The two "L" blocks, which conforms the specimen, were separated from each other when the push-off test finished. The aim of this operation was to study the resulting crack

surface.

It can be seen (Fig. 11) that the crack surface depends on the type of sand used. Thus, the river sand tends to form a soft surface, while the crush sand tends to form a rough one. This is independent of the type of fiber, because the specimen made with BN fibers shows a quite similar crack surface compared to the specimen with BP fibers.

a)

b)

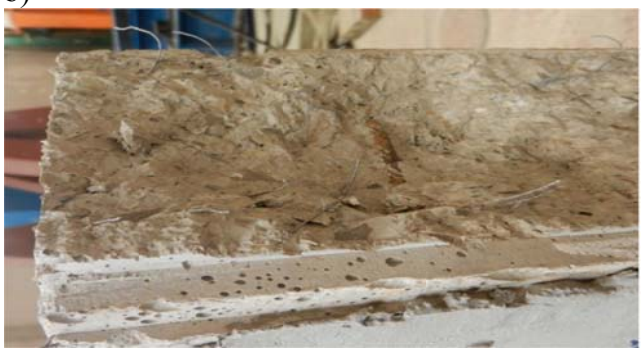

c)

Figure 15: Crack surface. a) River sand. b) Crush sand with BN fiber. c) Crush sand with BP fiber.

6 CONCLUSIONS

It is worth noting that the conclusions obtained in the present study are from preliminary results. This is because the specimens were used to detect and solve the different problems that present this new methodology.

The first problem was during the pre-crack process, because the specimen tends to rotate about the line load. To solve this problem the specimen was placed in a more rigid frame, and a better way to put in place the specimen was designed.

The other serious problem was to measure, with a certain grade of precision, the crack width. At the beginning, the readings of the LVDT's were not enough, because differences between them were detected, and it was hard to check them. Now, with the use of the microscope, there is another way to measure the crack width to compare and to obtain a better precision. More tests must be carried out to be sure of the precision of this technique.

Different behaviors and post-cracking responses have been detected depending on the type of fibers and the mix design. Also, these differences are more evident at high value of slip.

Finally, it is intended to develop a material model in order to take into account the crack behaviour with the experimental results obtained. The mechanisms of shear transfer to be considered will be the steel fibres, the aggregate interlock, and the dowel action due to the transverse reinforcement. The displacements to be included are the slip of the crack Δ and the crack width w, as well as the normal stress σ and the shear stress τ in the crack.

REFERENCES

[1] Khaloo, A.R. and Kim, N, 1997. Influence of Concrete and Fiber Characteristic on Behavior of Steel Fiber-Reinforced Concrete under Direct Shear, *ACI Journal, V. 94, No. 6*, November-December, 1997.

[2] Cuenca, E. and Serna, P., 2010. Shear Behavior and Mode of Failure analysis of different structural elements made with Fiber Reinforced Concrete, *8th fib PhD Symposium* in Kgs. Lyngby, June 20-23, 2010, Denmark.

[3] Cuenca, E. and Serna, P., 2010. Respuesta frente a cizallamiento en probetas tipo Z fabricadas con HACs de diferente estructura granular, *2º Congreso Ibérico sobre Hormigón Autocompactable,* 1 y 2 de julio, 2010, Guimarães.

[4] Valle, M. and Büyüköztürk, O., 1993. Behavior of Fiber Reinforced High-Strength Concrete under Direct Shear. *ACI Material Journal, V. 90, No. 2, March-April,* 1993.

[5] Hofbeck, A., Ibrahim, I. O. and Mattock, A. H., 1969. Shear Transfer in Reinforced Concrete. *Title No. 66-13, ACI Journal*, 196, pp. 119-128.

[6] Paulay, T. and Loeber, P. J., 1974. Shear Transfer by Aggregate Interlock. *Publication SP ACI, Vol. 42, Part V 1*, 1974, pp. 1-15.

[7] Walraven, J. C., 1981. Fundamental analysis of aggregate interlock. Journal of Structural Division, Vol. 107, No. 11, November, 1981. pp. 2245–2270.

[8] Taylor, H. P. J., *Investigation of the forces carried across cracks in reinforced concrete beams in shear by interlock of aggregate*, Cement and Concrete Association, London, 22, 1970.

[9] Walraven, J. C. and Stroband, J., 1994. Shear Friction in High-Strength Concrete. Publication SP ACI, Vol. 149, 1994. pp. 311-330.

[10] Young Hoon Kim, et al., 2010. Shear Characteristics and Design for High-Strength Self-Consoliding *Concrete. Journal of Structural Engineering. Vol. 136, No. 8, August, 2010. ASCE. 2010*. pp. 989-1000.

[11] Cuenca, E. and Serna, P., 2010. Comportamiento a cortante de vigas prefabricadas con hormigón tradicional y hormigón autocompactable. *2º Congreso Ibérico sobre Hormigón Autocompactable,* 1 y 2 de julio, 2010, Guimarães.

[12] Choulli, Y., et al., 2007. Comportamiento a esfuerzo cortante de vigas prefabricadas pretensadas de hormigón autocompactante de alta resistencia. *Hormigón y acero, ISSN 0439-5689, Num. 244*, 2007. pp. 47-56.

[13] Cuenca, E. and Serna, P., 2010, Shear behavior of self-compacting Concrete and Fiber Reinforced concrete Push-Off Specimens. *Design, Production and Placement of Self-Consolidating Concrete, RILEM Bookseries Volume 1*, 2010. Pp. 429-438

[14] Boulekbache, B., Hamrat, M., Chemrouk, M., Amzine, S., 2012. Influence of yield stress and compressive strength on direct shear behavior of steel fibre-reinforced concrete. Construction and Building Materials, Vol. 27, February, 2012. pp. 6-14. 2012.